

Electro–Opto–Thermal Modeling of Threshold Current Dependence on Temperature

D. S. Ellis, *Student Member, IEEE*, and Jimmy M. Xu, *Senior Member, IEEE*

Abstract—A self-consistent model of semiconductor quantum-well (QW) lasers is presented and deployed here for the study of threshold current dependence on temperature. The simulated dependencies of threshold current-density on temperature and cavity lengths agree well with experiments published by Evans *et al.* Aided with detailed knowledge so obtained of each contributor to the threshold current, attempts are made to gain insights into the well-known Pankove and other newly proposed empirical relations. The relative importance of the various mechanisms are evaluated, and self-heating is shown as an important factor determining the threshold current at high temperature.

Index Terms—Modeling, quantum-well lasers, semiconductor lasers, simulation, SPICE, temperature, threshold current.

I. INTRODUCTION

THRESHOLD current versus temperature is an important issue which has been widely investigated. The temperature dependence of threshold current has been empirically described by the well-known exponential Pankove [2] relation via the use of two parameters T_0 and I_0 , known as the characteristic temperature and the characteristic current. This relation is in general agreement with experimental observations and has been used extensively for its simplicity. However, it is known that T_0 is not strictly constant with temperature [3]. Recently, an alternative, but also empirical three-parameter formula was proposed by our colleagues based on a very large set of experimental data they measured in InP lasers [1]:

$$J_{\text{th}} = \left[\frac{n}{C} (T_{\text{max}} - T) \right]^{-1/n} \quad (1)$$

where $n \sim 0.5$, which was found to vary little with the cavity length and strain, T_{max} is the temperature of infinite threshold current, and C a device-dependent constant. A helpful insight for comparing the empirical J_{th} versus T relation of (1) to the also empirical exponential Pankove relation is that when the exponential and the inverse-power relations are expanded into Taylor series, the zeroth-, first-, and second-order terms of T/T_0 are almost identical (for the simplifications $n \sim 0.5$ and $T_0 \sim T_{\text{max}}/2$), but the higher order terms of the exponential function drop off much faster than those of the inverse power. This explains the commonality in low and medium temperature, and the difference in the high-temperature regime between the two functionalities.

Manuscript received December 3, 1996; revised February 28, 1997. This work was supported by the OLLRC, Nortel, and NSERC.

The authors are with the Department of Electrical and Computer Engineering, University of Toronto, Toronto, ON, M5S 1A4 Canada.

Publisher Item Identifier S 1077-260X(97)04519-X.

Nevertheless, the all important question of why J_{th} depends on T in this (or other) way remains largely unanswered. A more recent and well thought out investigation [4] reported thoroughly on the sensitivity of fundamental variables (such as gain and chemical potential) in the laser with temperature and with each other using both experimental results and a detailed model. Gain variation was identified as the dominant mechanism determining threshold current variation with temperature. However, for a given level of gain, even supposing that the required carrier concentration increased with temperature at the same rate for two different laser structures, the threshold current variations with temperature could still be very different. The complexity of the problem calls for a self-consistent treatment of the electro-opto-thermal interactions. Despite the usefulness and accuracy of the two-dimensional (2-D) self-consistent numerical model we have available [5], the issue is better handled by a model that, while sacrificing some detail and even depth, allows us to explore individually but self-consistently, the effects of numerous contributing mechanisms and examine their relative importance.

We present a lumped element model (named OE^{UT}-Spice), which builds on the work initiated in our lab a few years ago [6], for the electro–opto–thermal interactions within a laser and also for use in optoelectronic integrated circuit (OEIC) simulations. It is derived from first principle equations and can model the laser operation from below threshold to high injection levels. Moreover, it is self-consistent, with a reasonable CPU time, and does not have to assume the absence of self-heating or thermal impedance, which are significant above threshold and even at threshold for high threshold and high voltage lasers such as those with low carrier mobility materials (GaInP, GaN, etc.). To our own surprise and contrary to perhaps popular belief, self-heating and thermal dissipation rate turned out important at threshold even for high carrier mobility materials such as GaAs and InP as it will become evident later. Not to discount 2-D effects such as lateral spread of current and heat flow, approximations for these 2-D effects developed in the literature are drawn from for use in the lumped element model. For easy adoption by future users, the model is implemented in Spice-compatible format by introducing equivalent optical, electrical and thermal subcircuits. Unlike previous Spice-based and similar one-dimensional (1-D) models, we include, in addition to self-heating, almost all known important mechanisms that contribute to the T -dependence of I_{th} . These include the optical losses (material losses, free carrier/intervallence band absorption in the active region and cladding layers), mirror

losses, radiative (stimulated and spontaneous) and nonradiative (Auger, SRH) recombination with temperature and bandgap dependent coefficients, drift and diffusion leakage current, lateral current spreading, self-heating, and bandgap shrinkage with temperature and carrier concentration. Most of the material parameters are pre-calculated using a collection of equations and fits from the literature [7]–[9]. Only a few device structure dependent parameters are adjustable but will too be fixed after the calibration run. Given the abundance of data already in the literature, we will not be tempted to present yet more experimental measurements of $I_{\text{th}}(T)$ that we have. Instead, we will try to evaluate the relative importance of the related mechanisms and their dependencies on temperature, and thereby gain insights to the functional dependence of the overall current on temperature.

II. THE MODEL

Our model, derived from the integral form of first principle equations of drift-diffusion, thermal conduction, and photon rate, is expressed as equivalent optical, electrical and thermal circuits. The optical circuit's equivalent voltage is the optical power from the output facet. For the symmetric case of equal reflectivities,

$$P_{\text{opt}} = \frac{c_0}{2nl} S V_{\text{mode}} \ln\left(\frac{1}{R}\right) E_{\text{ph}} \quad (2a)$$

where c_0/n is the group velocity v_{gr} , l is the cavity length, V_{mode} is the effective mode volume in which S is the average photon density, E_{ph} is the energy per photon, and $\ln(1/R)$ is the transmission probability through the output facet. Note that $V_{\text{mode}}/l = A_{\text{active}}/\Gamma$, where A_{active} is the cross section of the active region perpendicular to the longitudinal axis and Γ is the confinement factor. This is the reduction of a more general expression which solves the boundary conditions at the two facets [10]. The above expression is modified in the model for the more general case of unequal mirror reflectivities [10]:

$$P_{\text{opt}} = \frac{c_0}{2nl} S V_{\text{mode}} E_{\text{ph}} \frac{(1-R_2)\sqrt{R_1}}{(\sqrt{R_1} + \sqrt{R_2})(1 - \sqrt{R_1 R_2})} \cdot \left[\ln\left(\frac{1}{R_1}\right) + \ln\left(\frac{1}{R_2}\right) \right] \quad (2b)$$

where R_2 is the reflectivity of the output facet. The symmetric case will be assumed for simplicity in the following equations.

Rearranging the terms of (2a),

$$S = \frac{2\Gamma P_{\text{opt}}}{v_{gr} A_{\text{active}} E_{\text{ph}} \ln(1/R_2)} \quad (3)$$

The rate equation for the photon density S begins as

$$\begin{aligned} \frac{dS}{dt} &= \frac{\partial S}{\partial t} + \frac{\partial S}{\partial z} \frac{\partial z}{\partial t} \\ &\Rightarrow \frac{dS}{dt} = \Gamma\beta R_{\text{sp}} + (\Gamma g_m(1 - \varepsilon S) - \alpha_{\text{loss}}) v_{gr} S \end{aligned} \quad (4)$$

where β is the fraction of spontaneous emission going into the lasing mode, R_{sp} is the spontaneous emission rate ($\text{cm}^{-3} \text{s}^{-1}$), g_m is the material gain (cm^{-1}), ε is the gain compression factor and α_{loss} is the loss (cm^{-1}). ε should be chosen carefully so as to distinguish itself from self-heating and free-carrier absorption effects [13]. From (3) and the gain term in the time derivative of photon density in (4), the expression for the stimulated radiative current in terms of the output power is

$$I_{\text{stim}} = \frac{2qlg_m\Gamma}{E_{\text{ph}} \ln\left(\frac{1}{R_2}\right)} P_{\text{out}} \cdot \left(1 - \frac{\varepsilon 2\Gamma P_{\text{out}}}{A_{\text{active}} v_{gr} \ln\left(\frac{1}{R_2}\right) E_{\text{ph}} q} \right) \quad (5)$$

where q is the electronic charge, and has been added to the last term for consistent units. Also, the spontaneous radiative current is

$$I_{\text{spon}} = q A_{\text{active}} l R_{\text{sp}} \quad (6a)$$

where

$$R_{\text{sp}} = Bn^2 = B_0 \left(\frac{T_0}{T} \right) \left(1 - \frac{n}{N^*} \right) n^2 \quad (6b)$$

where n is the electron concentration in the active region (in cm^{-3}), and $B(T, n)$ is the bimolecular recombination coefficient which is inversely proportional to T and decreases with n , following the treatment by Grinberg [11]. The functionality of (6b) matches excellently with calculated spontaneous lifetimes reported in Menzel *et al.* [12] Expressing the optical power from the output facet in terms of the spontaneous and stimulated radiative currents, substituting (3), (5), and (6) into (4) yields the desired optical equivalent circuit equation, upon rearrangement of terms in (7) found at the bottom of the page where α_i are the internal losses, σ_{2D} is the free carrier absorption cross section in the QW, σ_{3D} is the free-carrier

$$\frac{1}{l} \left(\frac{E_{\text{ph}}}{q} \right) I_{\text{stim}} + \frac{\beta}{l} \left(\frac{E_{\text{ph}}}{q} \right) I_{\text{spon}} = \frac{P_{\text{out}}}{R_{\text{opt}}} + C_{\text{opt}} \frac{dP_{\text{out}}}{dt} \quad (7a)$$

$$R_{\text{opt}} = \frac{\ln\left(\frac{1}{R_2}\right)}{2\alpha_{\text{loss}}} = \frac{\ln\left(\frac{1}{R_2}\right)}{2\left(\alpha_i + \frac{1}{2l} \ln\left(\frac{1}{R_1}\right) + \frac{1}{2l} \ln\left(\frac{1}{R_2}\right) + \Gamma\sigma_{2D}n + (1-\Gamma)\sigma_{3D}kn_b\right)} \quad (7b)$$

$$C_{\text{opt}} = \frac{2}{v_{gr} \ln\left(\frac{1}{R_2}\right)} \quad (7c)$$

absorption cross section in the bulk, and κn_b is the average bulk carrier concentration in the volume encompassed by the optical mode. As shown in Mikhaelashvili *et al.* [13], free carrier/intervale band absorption in the barrier and cladding regions becomes important, especially at higher temperatures, due to the higher volume and absorption cross section of 3-D carriers, and the accumulation of carriers outside the active region due to well-barrier hole burning (the latter is an effect of finite capture and escape times between well and barrier, causing damping in the transient step response [14], existing elsewhere in SPICE models [15], [16] but not concerned in this present investigation). R_{opt} and C_{opt} are the equivalent optical resistance and capacitance. The resultant equivalent sub-circuit model is shown in Fig. 1(a).

The material gain is calculated based on the quasi-Fermi levels with the gain formula outlined in Yan *et al.* [17].

$$g(E)$$

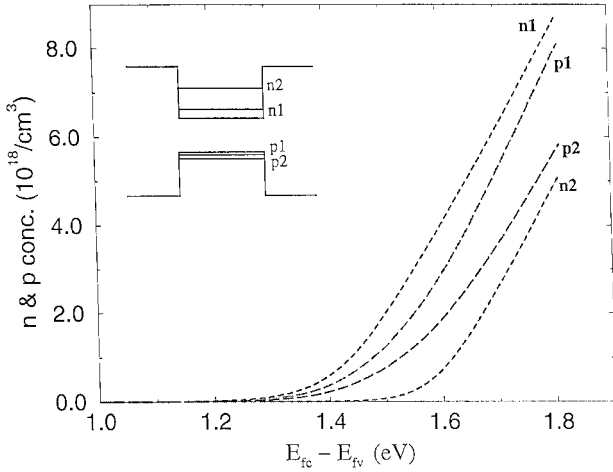


Fig. 2. Calculated carrier concentrations of the first two conduction band ($n1$ and $n2$) and valence band ($p1$ and $p2$) sub-levels of a 0.1-nm GaAs-AlGaAs QW at 300 K, as a function of quasi-Fermi level difference.

where $E_{fc\text{high}}$ is the asymptotic solution to (8) for $\exp((E_{fc} - E_{c1})/kT) \gg 1$, $E_{fc\text{low}}$ is for $\exp((E_{fc} - E_{c1})/kT) \ll 1$, W_{high} and W_{low} are weighting functions, and p and q are correction constants empirically refined beforehand by successive comparisons of $E_{fc0}(Vn, T)$ and the actual solutions. Although only the first conduction sub-band and first two valence heavy-hole sub-bands are considered in this calculation, this is justifiable in light of the populations of the bands involved. To illustrate the relative importance of the various sub-bands, the calculated populations of the first two conduction band and heavy hole sub-bands in GaAs are shown in Fig. 2. It is indeed seen that over the voltage range near threshold (~ 1.4 V) the second conduction sub-band of the QW has a much lower population compared to the first conduction sub-band and first two valence sub-bands.

The electrical equivalent sub-circuit is shown in Fig. 1(b). All of the current sources depend on carrier concentration, which in turn depend on the quasifermi levels, which are the solution to (9). The radiative recombination currents are from (5) and (6). The nonradiative recombination paths considered are the SRH and Auger recombinations, whose combined currents are expressed by

$$I_{NR} = ASRHn + C_{Aug}n^3. \quad (11)$$

The dominant Auger recombination processes are dependent on the material. Where band to band Auger processes are dominant, which is the case in InGaAsP [19], the coefficient C in the QW varies as

$$C_{Aug} \sim \sqrt{\frac{kT}{aE_g}} \exp\left(\frac{-(a-1)(E_g - \delta)}{kT}\right) \quad (12)$$

where a is the effective mass pre-factor relating the threshold energy for the process to the bandgap, δ is either zero or the split-off energy, depending on the Auger process [19], [20]. Such relations are used to assess the effects of both composition variations and temperature changes on the Auger coefficient.

The drift and diffusion leakage current is calculated via the approach in Chinn *et al.* [21], where the solution to the minority carrier diffusion equation in an electric field, given the boundary conditions of carrier density at the cladding layer edge and at the ohmic contact, resulted in the formula

$$I_{\text{leak}} = qAD_n n_b \left[\sqrt{\frac{1}{L_n^2} + \frac{1}{4z^2}} \text{Coth}\left(\sqrt{\frac{1}{L_n^2} + \frac{1}{4z^2}} t_{\text{clad}}\right) + \frac{1}{2z} \right]. \quad (13)$$

Here A is the area of carrier flow into the cladding region, t_{clad} is the cladding layer thickness, D_n is the temperature dependent diffusion constant, n_b is the number of electrons at the p-cladding layer edge, L_n is the diffusion length, and

$$z = \left(\frac{kT}{q}\right) \frac{\sigma}{J_{\text{tot}}}$$

where σ is the conductivity, and J_{tot} is the total current density through the p-cladding layer. For an $\text{Al}_x\text{Ga}_{1-x}\text{As}$ cladding layer, n_b is calculated as the sum of the concentrations in the Γ , X , and L bands, using bandgap and density of states effective mass data [7], [22]. The barrier heights relative to the conduction band edge in the well are approximated to be the sum of the conduction band discontinuities between the well and barrier, and barrier and cladding layer, which in this simulation are constant although more rigorous treatments exist [23]. Another approximation is that hole leakage is ignored due to the low-hole mobilities. Mobilities and diffusivities in the barrier are assumed to be an average, based on empirical data for various alloy compositions, and decrease accordingly with doping and temperature.

Another contributor to the total injected current arises from the lateral spreading of carriers away from under the ridge. The formula used to approximate the lateral current spreading was adopted from Yonezu *et al.* [24], where the incremental decrease in the lateral current due to downward flow through the p-n junction, combined with the lateral voltage drop, are combined to form a differential equation. The resultant total spreaded current is expressed as a function of the current injected into the active region:

$$I_{\text{spread}} = 2\sqrt{\frac{2t_{\text{clad}}l\sigma_y}{W_{\text{ridge}}}\left(\frac{kT}{q}\right)} I_{\text{unspread}} \quad (14)$$

where t_{clad} , l , and W_{ridge} are the p-cladding layer thickness, cavity length and ridge width respectively, σ_y is the effective lateral conductivity under the ridge, and I_{unspread} is the total current going into the active region (the sum of the current components described above). For a higher degree of accuracy, there are more detailed studies of lateral current confinement in ridge structures [25], [26], but (14) was found to give a reasonable assessment of injection efficiency compared to independent calculations [27] given a proper value of σ_y .

Self-heating in an individual laser is accounted for with the lumped element equivalent subcircuit for the thermal system, based on the heat flow equation [6], which in integral form

results in

$$G_{\text{tot}i} = \frac{\Delta T_{ij}}{\mathcal{R}_{ij}} + C_i \frac{dT_i}{dt} \quad (15)$$

where

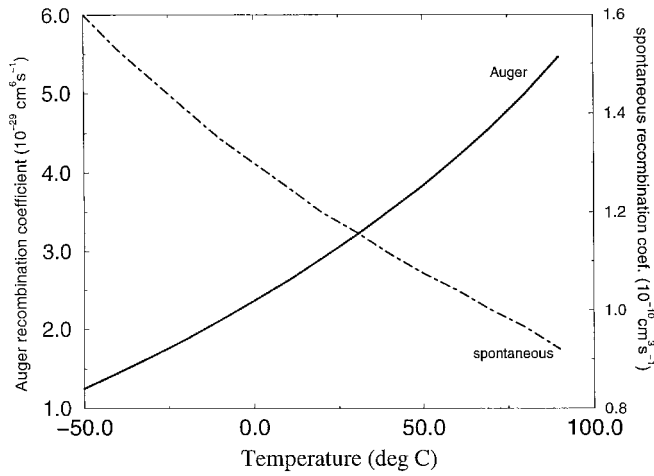


Fig. 4. Calculated (a) Auger and (b) spontaneous recombination coefficients used in the simulation for the InGaAsP QW laser at laser threshold versus heat sink temperatures temperature.

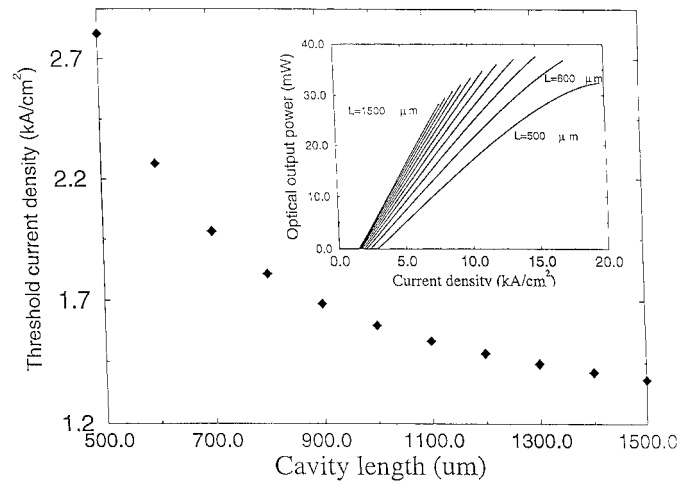


Fig. 6. Inset: simulated L - J curves at 20 °C for cavity lengths from 500 μm to 1500 μm . Foreground: calculated threshold current density versus cavity length at 20 °C.

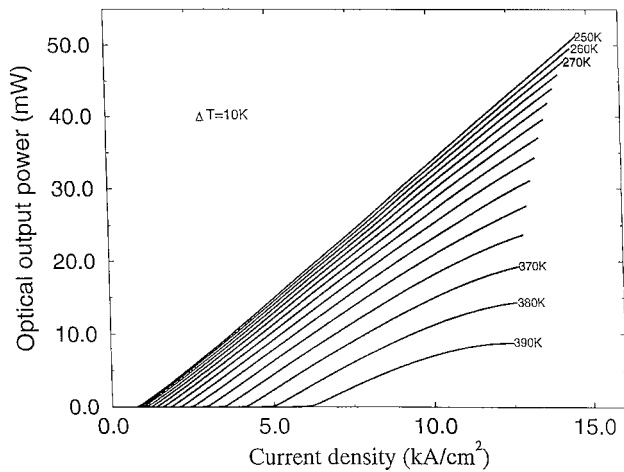


Fig. 5. Optical output power versus threshold current density simulating the 800- μm -long R1-400 InGaAsP laser at heat sink temperatures ranging from -50 °C to 90 °C.

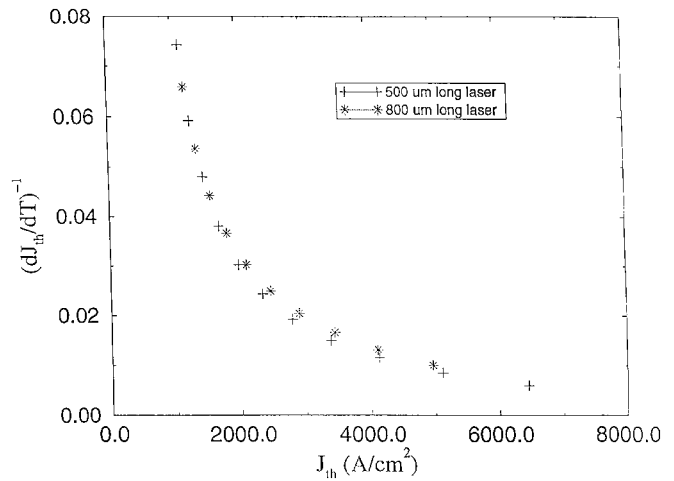


Fig. 7. $(\partial J_{th}/\partial T)^{-1}$ versus J_{th} calculated for both the 800- μm and 500- μm -long InGaAsP lasers.

the experiments of Evans *et al.*, and results in a reasonable value of injection efficiency [27]. The spontaneous emission coupling coefficient β was 1×10^{-3} . The gain compression coefficient ϵ used was $3 \times 10^{-18} \text{ cm}^3$.

The simulated L - J characteristics for different temperatures of the unstrained InGaAsP three 6.4-nm QW lasers is shown in Fig. 5. The inset Fig. 6 is a set of L - J curves for different cavity lengths whose threshold values are shown in the figure itself, which is in very good quantitative agreement with [1]. The ridge width in all of the lasers is 2 μm . To verify that this model reproduces qualitatively, the other aspects of the experimental results of Evans *et al.* [1], a plot of $(\partial J_{th}/\partial T)^{-1}$ versus J_{th} , for two considerably different cavity lengths, is shown Fig. 7. As experimentally observed by Evans *et al.* [1], the set of points for two different cavity lengths lie on the same curve. Fig. 8 shows the J_{th} versus sink temperature relation for cavity lengths of 500 and 800 μm . Our best fits of (1) to those curves indicated that $n = 0.38$ and 0.42 for $L = 800 \mu\text{m}$ and $L = 500 \mu\text{m}$, respectively, compared to experimental $n \sim 0.5$. Obtaining Pankove's characteristic temperature T_0

from the gradient of the computed J_{th} - T curves is shown in Fig. 9. As found in [1], the curves are fairly parallel for different cavity lengths, due to the fact that n is the same.

The advantage of this self-consistent lumped element circuit approach includes the ability to separately follow the behavior of each individual effect. Playing a key role in each of these individual effects, however, is the carrier concentration at the threshold gain (even if it too is a variable) for a given temperature. This relation was found to be approximately linear with temperature for both the GaAs and InGaAsP QW lasers simulated.

The various current components of the 800- μm QW laser at threshold are plotted in Fig. 10 (excluding SRH recombination which was found to be relatively small). Although the noncaptured current component is displayed, it is a fraction of the total captured current and will not be considered in the actual comparisons albeit it is an important issue in itself. From about 0 °C to 30 °C the leakage, Auger recombination and spontaneous recombination components are of the same order of magnitude, in the sense that one is not larger than

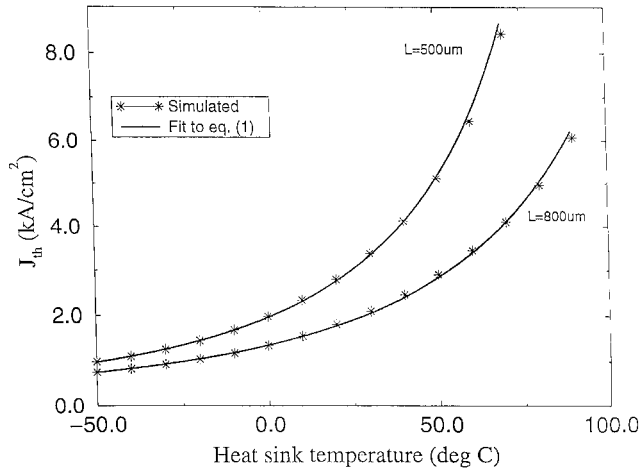


Fig. 8. Threshold current density versus heat sink temperature: the simulation and its fits to (1) for cavity lengths of 500- and 800- μm InGaAsP QW lasers.

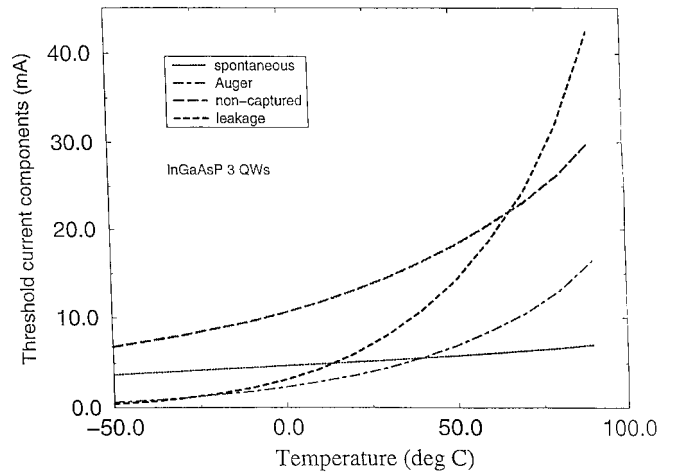


Fig. 10. Threshold current components versus temperature of the 800- μm -long InGaAsP laser. Included is the Auger recombination current, spontaneous recombination current, over-barrier spillage (leakage) current and laterally spreaded (noncaptured) current.

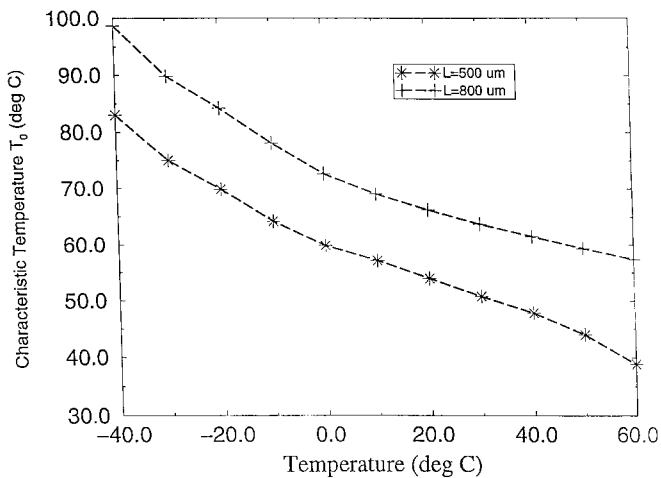


Fig. 9. Characteristic temperature T_0 versus heat sink temperature derived from the simulations for the 500- and 800- μm -long lasers.

the sum of the other two. Spontaneous threshold current, while in this temperature range is one of the significant contributors, has the slowest gradient with temperature, and at below 0 °C is clearly the dominant threshold current component. This is consistent with the observed near linear $I_{th}-T$ dependence in experiments in that temperature range. The slow increase of threshold spontaneous recombination current with temperature (at a rate less than $T^{3/2}$) is attributed to the decrease of the spontaneous recombination coefficient with both increasing temperature and carrier concentration, as in (6b) and Fig. 4. Likewise, the Auger coefficient of (12) and Fig. 4 increases superlinearly with temperature resulting in the increasing importance of Auger recombination over spontaneous recombination current with increasing temperature. In addition, the Auger recombination current has a cubic rather than quadratic dependence on carrier concentration. Finally, it is seen that over barrier leakage is the most prominent threshold current component at high temperature (above 30 °C). This latter conclusion is qualitatively identical to that reached by Bernussi *et al.* [30] for typical strained InGaAsP

QW lasers. The consequence is that for high temperatures the temperature sensitivity would depend heavily on the cladding layer properties. A higher energy gap of the cladding material should reduce the n_b term of (13), but would also decrease the mobility and hence increase the resistance, power dissipated, and heating, which as will be seen can have a critical effect on the temperature dependence of threshold current. The confinement factor would also be a variable in this case. It should be possible to minimize the over-barrier leakage by careful quantitative optimization procedure.

The values of T_{max} obtained from these results deviate somewhat from the experimental results [1]. Our simulations indicated that laser operation for the particular 500- μm laser became impossible at ~ 80 °C, while the experimentally extrapolated result for T_{max} is ~ 105 °C [1]. However, as offered in [1], the $J_{th}-T$ characteristic, including the value of n , is highly dependent on thermal resistance and in addition, ohmic resistance is of almost equal importance due to Joule heating. It could very well be that the effective thermal and/or ohmic resistance was overestimated on our part (for one thing, we opted not to take into account the effect of doping on the thermal conductivity of the various layers and the contribution of the spreaded current component to the overall Joule heating was perhaps overestimated). We suggest that the physical origin of T_{max} in the newly proposed empirical relation (1) is the temperature beyond which, at some point prior to reaching the threshold gain, attempting to increase the carrier concentration results in such an increase in self heating that in fact the gain is lowered rather than increased with increased carrier concentration. This process is illustrated in Fig. 11 in the case of a laser at high temperature which will never reach threshold. In the case of the 500- μm laser at a sink temperature of 70 °C, the simulated active region temperature at threshold, a key factor in determining the value of n , becomes 90 °C (for the parameters used in the simulation), which is a very significant rise in temperature, and indeed involves the “complex feedback mechanisms” speculated in [1]. Although this self-heating effect we likely

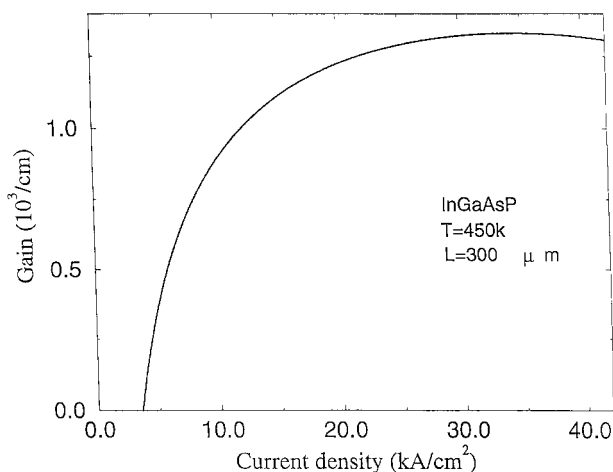


Fig. 11. Subthreshold gain versus current-density for a 300- μm -long InGaAsP laser operating at 150 $^{\circ}\text{C}$. The maximum in the gain curve indicates that lasing threshold will never be reached.

over-estimated as explained above, this just means that it becomes more important at higher temperatures than we predicted. In fact, upon making corrections in the thermal sub-circuit with respect to thermal resistance and laterally spread current, the simulated threshold temperature rise at 70 $^{\circ}\text{C}$ is indeed only 2 $^{\circ}\text{C}$, but at a sink temperature of 100 $^{\circ}\text{C}$, the at-threshold temperature rise of 7 $^{\circ}\text{C}$ takes on significance again. It should be pointed out that an additional effect which could result in a similar positive feedback situation with respect to increasing the threshold carrier concentration, is free-carrier absorption in the inner barriers [31], which was not presently explored with this model due to lack of reasonably precise knowledge of this effect in the literature (but could be incorporated into the model the same way as free carrier absorption in the cladding layer, given the quasi-Fermi levels and barrier heights). However, as seen in papers such as [4] and [13] it is a significant effect. We are not presently sure if this effect would result in the relation of equation (1) as does the self-heating effect. Other mechanisms, included in the simulation, such as the increase of Auger coefficient and thermal resistance with temperature also come into play to compound these effects. On the basis of the model presented here, improvements and additions, informed by the recent findings such as [4] can be pursued.

IV. SUMMARY

The simulation results using the lumped-element model of QW semiconductor lasers were in good agreement with published experimental results, for GaAs and InGaAsP based lasers and with the empirical threshold current versus temperature functionalities of Pankove and Evans *et al.* The various contributors to these relations, once combined in the self-consistent simulation, were individually accessed for their overall relative importance in different temperature ranges. In the case of the GaAs laser, it is confirmed that spontaneous emission component is the dominant factor of threshold current from low (below room temperature) up to high temperature ranges (over 400 K). In the case of InGaAsP, there is no

one clear dominant loss mechanism at temperatures around $\sim 0^{\circ}\text{C}$ –30 $^{\circ}\text{C}$ as the competing effects of spontaneous recombination, Auger recombination, and leakage current are on an approximately equal basis, but the rate of change of spontaneous recombination current with temperature is the slowest. At higher temperatures, leakage current becomes the primary current component. It is clear that for high power and high temperature operations, measures in laser design must be devised to suppress the over barrier leakage but without suffering excessive additional heating and degradation to mode quality. Regardless of the loss mechanisms of carriers in the active region, injection efficiency and its variation with temperature is a significant factor. For CW operation, self-heating effects become significant for threshold current at high temperatures, and should self-consistently be included in the laser model.

ACKNOWLEDGMENT

The authors express their gratitude to A. Tager for invaluable discussions, and scrutiny of several aspects of the physical model. Equal thanks to N. Bewtra and D. Suda for providing the basis for this work and advice on the finer points of Spice, G.-L. Tan for helping us with material data, H. Chikh for proof reading the paper, and to Dr. T. Makino for encouraging us to engage in this subject.

REFERENCES

- [1] J. D. Evans, J. G. Simmons, D. A. Thompson, N. Puetz, T. Makino, and G. Chik, "An investigation into the temperature sensitivity of strained and unstrained multiple quantum-well, long wavelength lasers: New insight and methods of characterization," *IEEE J. Select. Topics Quantum Electron.*, vol. 1, pp. 275–284, June 1995.
- [2] J. I. Pankove, "Temperature dependence of emission efficiency and lasing threshold in laser diodes," *IEEE J. Quantum Electron.*, vol. QE-4, pp. 119–122, 1968.
- [3] A. F. J. Levi, J. O'Gorman, S. Schmitt-Rink, T. Tabun-Ek, D. G. Coblenz, and R. A. Logan, "Temperature dependence of semiconductor lasers," in *SPIE, Physics and Simulation of Optoelectronic Devices*, 1992, vol. 1679, pp. 85–95.
- [4] D. A. Ackerman, G. E. Shtengel, M. X. Hybertsen, P. A. Morton, R. F. Kazarinov, T. Tanbun-Ek, and R. A. Logan, "Analysis of gain in determining T_0 in 1.3 μm semiconductor lasers," *IEEE J. Select. Topics Quantum Electron.*, vol. 1, pp. 250–263, June 1995.
- [5] G.-L. Tan, N. Bewtra, K. Lee, J. M. Xu, "A two-dimensional non-isothermal finite element simulation of laser diodes," *IEEE J. Quantum Electron.*, vol. 29, pp. 822–835, Mar. 1993.
- [6] N. Bewtra, D. A. Suda, G. L. Tan, F. Chatenoud, J. M. Xu, "Modeling of quantum-well lasers with electro-opto-thermal interactions," *IEEE J. Select. Topics Quantum Electron.*, vol. 1, pp. 331–340, June 1995.
- [7] *Properties of Gallium Arsenide*, 2nd ed. U.K.: INSPEC, 1990, EMIS Data Rev. Ser. no. 2.
- [8] P. S. Zory, *Quantum Well Lasers*. Boston, MA: Academic, 1993.
- [9] B. A. Foreman, "Analytic model for the valence-band structure of a strained quantum well," *Phys. Rev. B (Condensed Matter)*, vol. 49, no. 3, pp. 1757–1773, Jan. 1994.
- [10] G. P. Agrawal and N. K. Dutta, *Long-Wavelength Semiconductor Lasers*. New York: Van Nostrand Reinhold, 1986, pp. 60–61.
- [11] A. A. Grinberg, "Approximate dependence of the spontaneous emission rate on electron and hole concentrations," *IEEE J. Quantum Electron.*, vol. 30, pp. 1151–1155, May 1994.
- [12] U. Menzel, A. Barwelff, P. Enders, D. Ackermann, R. Puchert, and M. Voss, "Modeling the temperature dependence of threshold current, external differential efficiency and lasing wavelength in QW laser diodes," *Semiconduct. Sci. Technol.*, vol. 10, no. 10, pp. 1382–1392, Oct 1995.
- [13] V. Mikhaelashvili, N. Tessler, R. Nagar, G. Eisenstein, A. G. Dentai, S. Chandrasakhar, and C. H. Joyner, "Temperature dependent loss and

- overflow effects in quantum well lasers," *IEEE Photon. Technol. Lett.*, vol. 6, pp. 1293–1296, Nov. 1994.
- [14] M. O. Vassell, W. F. Sharfin, W. C. Rideout, and J. Lee, "Competing effects of well-barrier hole burning and nonlinear gain on the resonance characteristics of quantum well lasers," *IEEE J. Quantum Electron.*, vol. 29, pp. 1319–1329, May 1993.
- [15] M. F. Lu, J. S. Deng, C. Juang, M. J. Jou, and B. J. Lee, "Equivalent circuit model of quantum well lasers," *IEEE J. Quantum Electron.*, vol. 31, pp. 1418–1422, Aug. 1995.
- [16] H. A. Tafti, F. N. Farokhrooz, K. K. Kamath, and P. R. Vaya, "Variation of threshold current with well barrier hole burning effect in quantum well lasers," in *SPIE*, 1995, vol. 2397, pp. 455–460.
- [17] R. H. Yan, S. W. Corzine, L. A. Coldren, and I. Suemune, "Corrections to the expression for gain in GaAs," *IEEE J. Quantum Electron.*, vol. 26, pp. 213–216, 1990.
- [18] P. Blood, S. Colak, A. I. Kucharshka, "Temperature dependence of threshold current in GaAs/AlGaAs quantum well lasers," *Appl. Phys. Lett.*, vol. 52, p. 599, 1988.
- [19] N. K. Dutta and R. J. Nelson, "The case for Auger Recombination in $\text{In}_{1-x}\text{Ga}_x\text{As}_y\text{P}_{1-y}$," *J. Appl. Phys.* 53(1), p. 74–92, Jan 1982.
- [20] A. Sugimura, "Comparison of band to band Auger processes in InGaAsP," *IEEE J. Quantum Electron.*, vol. QE-19, pp. 49–53, June 1983.
- [21] S. R. Chinn, P. S. Zory, and A. R. Reisinger, "A model for GRIN-SCH-SQW diode lasers," *IEEE J. Quantum Electron.*, vol. 24, pp. 2191–2214 Nov. 1988.
- [22] S. Adachi, "GaAs, AlAs and $\text{Al}_x\text{Ga}_{1-x}\text{As}$ material parameters for use in research and device applications," *J. Appl. Phys.*, vol. 58, no. 3, pp. R1–R29, Aug. 1985.
- [23] R. F. Kazarinov and M. R. Pinto, "Carrier transport in laser heterostructures," *IEEE J. Quantum Electron.*, vol. 30, pp. 49–53, Jan. 1994.
- [24] H. Yonezu, I. Sakuma, K. Kobayashi, T., Kamejima, M. Ueno, and Y. Nannichi, "A GaAs- $\text{Al}_x\text{Ga}_{1-x}\text{As}$ double heterostructure planar stripe laser," *Jpn. J. Appl. Phys.*, vol. 12., no. 10, pp. 908–915, Oct., 1973.
- [25] M.-C. Amann and W. Thulke, "Current confinement and leakage currents in planar buried-ridge-structure laser diodes on Si -substrate," *IEEE J. Quantum Electron.*, vol. 25, pp. 1595–1601, July 1989.
- [26] G. Beister, "Evaluation of electroluminescence current and voltage dependence in ridge waveguide laser structures," *Solid-State Electron.*, vol. 34, no. 11, pp. 1255–1262, 1991.
- [27] K. Lee, private communication.
- [28] L. A. Coldren and S. W. Corzine, *Diode Lasers and Photonic Integrated Circuits*. New York: Wiley, 1995, p. 56.
- [29] M. Ito and T. Kimura, "Stationary and transient thermal properties of semiconductor laser diodes," *IEEE J. Quantum Electron.*, vol. 32, pp. 787–795, May 1981.
- [30] A. A. Bernussi, J. Pikal, H. Temkin, D. L. Coblentz, and R. A. Logan, "Rate equation model of high-temperature performance of InGaAsP quantum well lasers," *Appl. Phys. Lett.*, vol. 66, no. 26, pp. 3606–3608, June 1995.
- [31] S. Seki, H. Oohashi, H. Sugiura, T. Hirono, and K. Yokoyama, "Study on the dominant mechanisms for the temperature sensitivity of threshold current in 1.3- μm InP-based strained-layer quantum-well lasers," *IEEE J. Quantum Electron.*, vol. 32, pp. 1478–1486, Aug. 1996.

D. S. Ellis (S'96), photograph and biography not available at the time of publication.

Jimmy M. Xu (M'87–SM'91), for a photograph and biography, see this issue, p. 512.